Understanding the mechanism by which nitrilotriacetic acid interacts with precipitating barium sulfate†

F. Jones,*[a] A. Oliveira,[a] A. L. Rohl,[b] M. I. Ogden[a] and G. M. Parkinson[a]

Received 12th June 2006, Accepted 3rd October 2006
First published as an Advance Article on the web 12th October 2006
DOI: 10.1039/b608302a

Morphology modifiers can act in many different ways on the precipitating phase. Inhibitors can alter the solution chemistry and thereby change the supersaturation, they may adsorb onto the surface and block growth and agglomeration, they may alter the critical nucleus and affect nucleation or they may do a combination of these three. Previous work showing that nitrilotriacetic acid (NTA) had a significant effect on barium sulfate precipitation has been expanded upon in order to determine the mechanism by which the observed morphology modification occurs. The absence of significant complexation to barium at the pH of the experiment suggests that NTA affects the critical nuclei of the precipitating barium sulfate. This results in the longer induction times observed using nephelometry, and adsorption onto growth features is probably the mechanism of interaction. Molecular modelling shows that NTA adsorption is favourable on terraces and that hydrogen bonding improves the ability of an additive to adsorb. A fundamental understanding of the mechanisms by which additives affect crystal growth is essential if new additives, with predictable effect, are to be designed *a priori*.

Introduction

Particle engineering is an important aspect of many industries[1–3] and much research has focussed on being able to 'tailor-make' or design additives which affect particle morphology in a predicted way.[4,5] Barium sulfate has often been used as a model compound since it is easy to control the precipitation conditions and it is an industrially important scale-forming compound.[6,7] Previous literature on aminocarboxylate additives has reported that they effect barium sulfate morphology.[8,9] These experiments were conducted at very high pHs (10–12) and at high carboxylate to barium ratios, resulting in chelation of the barium in solution. Work previously conducted by us has shown that the aminocarboxylate, nitrilotriacetic acid (NTA), not only affects barium sulfate precipitation at lower concentrations and pHs than those previously discussed, but also appears to interact with barium sulfate in a different manner to other inhibitors (phosphonates).[10]

In this study, both the morphology of the resultant barium sulfate particles and the kinetics of crystallization were assessed in order to determine the mode of interaction of NTA with barium sulfate.

The structure of this molecule is given in Fig. 1.

Experimental

The procedure consisted of monitoring crystallization using conductivity and nephelometry probes, while molecular modelling was undertaken to investigate the surface to additive interactions. Infrared (FTIR) spectroscopy, and microscopic techniques (SEM and TEM) were used to further support the mechanistic interpretation of the interaction of NTA with barium sulfate.

Conductivity

As described previously in ref 10, a stoichiometric amount of sodium sulfate was added to a barium chloride solution such that the final concentration was 0.25 mM. The temperature was 25 °C and the pH was 5.6 for experiments unless otherwise stated with the resulting initial supersaturation ratio ~25. The standard conditions result in rectangular crystals (Fig. 2a). The additive was added to the barium chloride solution prior to the sodium sulfate being added to start precipitation (final concentrations ranging from 0.007 to 0.078 mM), and the resultant particles were then filtered, washed and dried for SEM preparation. Due to the fact that supersaturation changes with time in batch crystallization runs such as these, the conductivity data are used to determine whether inhibition of the overall precipitation process occurs and whether there is any trend with additive concentration.

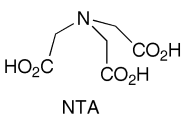

NTA

Fig. 1 Molecular structure of nitrilotriacetic acid, NTA.

[a]*AJ Parker CRC for Integrated Hydrometallurgy Solutions, Nanochemistry Research Institute, Department of Applied Chemistry, Curtin University of Technology, GPO Box U1987, Perth, WA 6845, Australia. E-mail: franca@ivec.org; Fax: (618) 9266 4699; Tel: (618) 9266 7677*
[b]*iVEC, 'The hub of advanced computing in Western Australia', 26 Dick Perry Avenue, Technology Park, Kensington, WA 6151, Australia*
† Electronic supplementary information (ESI) available: Molecular modelling. See DOI: 10.1039/b608302a

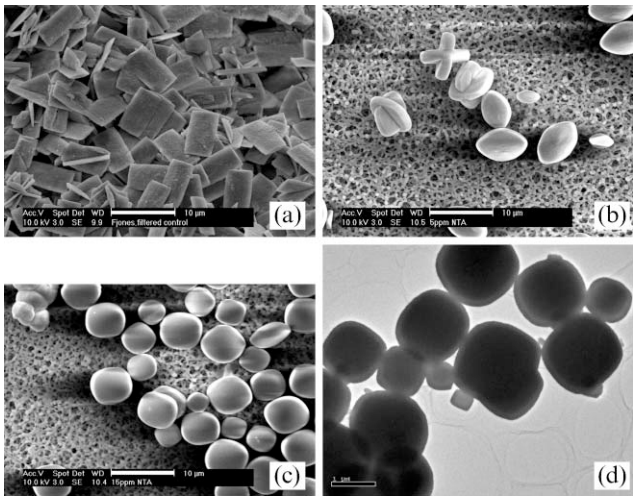

Fig. 2 Micrographs of barium sulfate particles obtained in the presence of (a) control—no additives (scale bar 10 μm); (b) 0.026 mM NTA (scale bar 10 μm); (c) 0.078 mM NTA (scale bar 10 μm); and (d) TEM image of particles produced with 0.078 mM NTA (from a 5 L batch, scale bar 1 μm).

Nephelometry

The method for nephelometry was the same as that for conductivity except for the probe used (conductivity *versus* nephelometry) and the speed of stirring. Stirring was at 300 rpm for the nephelometry experiment in order to ensure that a representative sample of particles came to the probe window and a reading automatically logged to a computer every 2 s. Nephelometry was used in order to determine whether NTA had an effect on the induction time (and therefore the nucleation rate) of barium sulfate precipitation. The increased scatter at the lower NTA concentrations could be due to the larger variation in particle size (*i.e.* size distribution) and the rectangular form of the particles themselves. At higher NTA concentrations the barite particles are (a) more uniform and (b) more spherical, and this may lead to less variation in the turbidity reading (which is susceptible to both particle number, shape and size effects[11]). The induction time has been calculated using an intersection of lines method given that there are various ways in which the induction time can be defined;[12] *i.e.* in this work, we have determined the baseline intersection point with the initial linear section. The error associated with this method was found to be $\sim \pm 20\%$.

Furthermore, a barite precipitation run in the presence of 0.26 mM NTA was performed where samples were taken during the experiment for transmission electron microscopy (TEM). A 10 μL sample of the suspension was placed on the TEM grid (carbon coated 200 Cu mesh) and the excess fluid was adsorbed by filter paper after 20 min (to allow particles to settle onto the grid). The samples were left to dry in a desiccator prior to viewing in a JEOL 2011 transmission electron microscope operated at 200 kV.

A 5 L batch of barium sulfate precipitated in the presence of 0.078 mM NTA was conducted in order to obtain sufficient solids for XRD and thermogravimetry.

Fourier transform infrared (FTIR)

Infrared spectra were obtained using the horizontal attenuated total reflection (HATR) accessory (a zinc selenide crystal) on a Bruker IFS 66 instrument. The resolution was 4 cm^{-1} and an MCT (mercury cadmium telluride) detector was used with an aperture of 12 mm. Barium sulfate with mean volume radius size (using Malvern Mastersizer) of $\sim$270 nm and 90% of particles below 560 nm (surface area was found to be 7.4 $m^2\,g^{-1}$ using N_2 adsorption and the BET isotherm model) was prepared as the solid substrate from analytical grade reagents. The NTA was prepared at 1 g L^{-1} at pHs 5, 6, 7 and 8 by adding the minimum volume of hydrochloric acid or sodium hydroxide required. 256 scans were obtained for all spectra. Approximately 1 mL of the solution (or slurry) was introduced on to the crystal surface using a Pasteur pipette and the crystal cleaned between solutions using milliQ water and ethanol. The optical pathway beneath the crystal was purged with dry nitrogen prior to analysis to remove as much carbon dioxide and water vapour as possible.

The adsorbed organic spectra were derived by subtracting the spectra of barium sulfate in solution at a given pH from the spectra of the organic and barium sulfate in solution at a given pH. The changes in the adsorbed spectra from the initial solution spectra show that the solution contribution is negligible.

Molecular modelling

Molecular modelling was undertaken using empirically derived potentials, most of which have been previously published.[13] Those potentials relating specifically to NTA are available in the ESI.† The GDIS[14] program was used for visualisation and setting up of the simulations and GULP[15] was used as the energy minimisation tool. The reader is directed to the references supplied[16,17] for further details regarding the methodology employed. Very briefly, once a surface and surface termination were selected, a sulfate was removed from the surface layer (to allow the system as a whole to remain uncharged, a necessary requirement in periodic systems) and the NTA molecule placed in a random orientation several Angstroms away from the surface. The system was then allowed to minimise its energy, which involves the additive docking into the surface. Many initial starting configurations were explored and different sulfate molecules were removed from the surface in an effort to find the global energy minimum. The replacement energy is then calculated, which is the difference in energy of the surface with adsorbed inhibitor to the energy of the pure surface taking into consideration the solvation of the inhibitor and the sulfate ions that are replaced.[13,16,17] Parameters used for the modelling are presented in the ESI.†

Results

As discussed previously,[10] NTA does show inhibition of barium sulfate precipitation (see Table 1). The concentration of NTA required to reduce the de-supersaturation rate by half is 0.078 mM, which is equivalent to 1 NTA molecule per 3 barium ions. That is, on a carboxylate to barium atom ratio, it is 1 : 1. The speciation curve (see Fig. 3) of NTA at pH 5.6 shows that the molecule would be in the LH^{2-} form (where L

Table 1 De-supersaturation rate and induction time calculated from conductivity and nephelometry experiments

NTA concentration in mM (ppm), ~L : M ratio	De-supersaturation rate[a]/−1 × 10^{-8} S cm^{-1} s^{-1}	Induction time/s[b]
0	3.34	250
0.026 (5.0), 1:10	3.85	659
0.039 (7.5), 1:6	NP	758
0.052 (10.0), 1:5	2.34	901
0.065 (12.5), 1:4	NP	905
0.078 (15.0), 1:3	1.33	1716

[a] From conductivity. [b] From nephelometry, NP = experiment not performed.

refers to the fully deprotonated ligand and H is hydrogen). The hydrogen, however, would be expected to be on the nitrogen as a zwitterion[18] and thus the NTA molecule actually has three fully deprotonated carboxylate groups all of which could interact with barium. The speciation curve, however, shows that actual complexation with barium is expected to be low at the concentrations used in this study and is at most 10% of the total NTA concentration for pHs less than 7. Further details of the speciation curves, the effect of NTA concentration and temperature can be found in the ESI (Fig. S1 and S2).†

Compare these results with Uchida *et al.*[8,9] (where they used a carboxylate/Ba ratio of 6 : 1). In our study the morphology changes begin to be observed at ratios of approximately 1 : 10 (carboxylate/Ba). As the concentration of NTA is increased, the particles become increasingly rounder and smaller particles can be observed (Fig. 2b and 2c). Some intergrown particles are also seen in Fig. 2b.

XRD of the particles formed in the presence of 0.078 mM NTA showed no significant line broadening when compared to the control sample.[10] The uniformity of the particles was found to be dependent on the hydrodynamic conditions (*i.e.* stirring conditions, flow patterns in the vessel) as shown by the TEM (Fig. 2d) and SEM (see ESI, Fig. S3)† picture of particles formed from a 5 L batch under the same chemical conditions. This is not unexpected and simply confirms that the hydrodynamic conditions of the small vessel were not completely replicated on scale up to 5 L. Particle sizing on a Malvern Zetasizer NanoZ for the solids produced from the 5 L batch sample gave a volume average size of 208 nm.

It was found that NTA in solution is susceptible to ageing effects over time (~1 month) and that, more importantly, the aged NTA did not affect the morphology of the precipitated barium sulfate. Thus, NTA decomposes and/or degrades over time in aqueous systems. Microbial degredation of NTA has been reported in the literature.[19]

Nephelometry results show that NTA increases the induction time of barium sulfate precipitation as the concentration of NTA increases (Fig. 4). Thus, NTA inhibits nucleation. The differences in the de-supersaturation rates and induction times observed with increasing NTA concentration are shown in Table 1. It must be remembered that the turbidity is determined by many factors other than particle number (including size and anisotropy) as discussed in the Experimental section and the important information gained from these data sets is the induction time for which there is a theoretical basis.[12] Thus, the crossing over of data between the 12.5 and 15 ppm samples could be due to: (i) errors in the method; (ii) fewer particles being observed by the turbidity meter (because the crystallization process has created fewer particles, agglomeration and/or as a result of subtle changes in the placement of the probe); (iii) the shape of the particles being measured; and (iv) the size of the particles being measured. It could also be a combination of these factors.

The issue of whether the NTA alters the solubility of barium sulfate by interacting even slightly with the barium cation can be excluded. We can see from the speciation curve of NTA (Fig. 3) that complexation with barium is minimal at the pH investigated here. Therefore, complexation effects can be ruled out.

Fig. 5 shows the change in the control morphology with temperature. Clearly, the particles become thicker (*i.e.* the (001) face appears larger) and the aspect ratio becomes smaller (and closer to 1) for the control particles of barium sulfate as temperature increases. This is expected, as the supersaturation decreases as temperature increases (when concentrations remain constant) and this is the expected morphology change with decreasing supersaturation.[20]

The barite particles formed in the presence of NTA change dramatically with temperature on going from 25 to 60 °C. The roughly spherical particles become rhombs reminiscent of the morphology of barite at very low supersaturations. The pH was found not to impact significantly on the morphology of

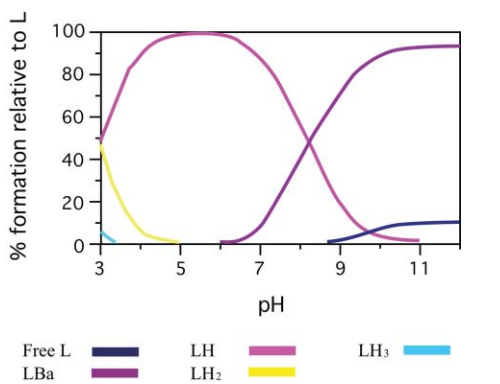

Fig. 3 Speciation curves for NTA. (Ligand, L, to metal ratio of 1 : 1 which is equivalent to 50 ppm or 0.26 mM NTA present.)

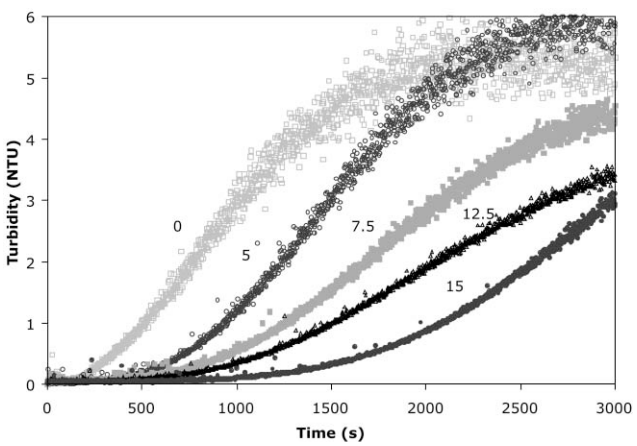

Fig. 4 Nephelometry results of barium sulfate precipitated in the presence of varying NTA concentrations (ppm).

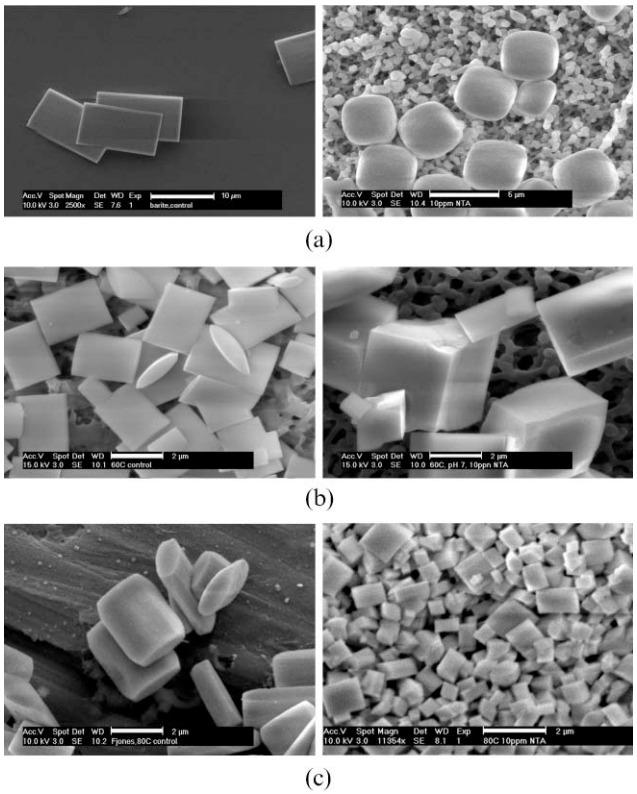

Fig. 5 Effect of temperature on morphology of barium sulfate particles formed (control and with 0.078 mM NTA). (a) 25 °C; (b); 60 °C; (c) 80 °C (all scale bars 2 μm, except top pictures which are 10 and 5 μm, respectively).

the barite particles formed in the presence of 0.052 mM NTA (see ESI, Fig. S4, particles shown were formed at pH 12)† at 25 °C.

Interestingly, the effect of pH on the de-supersaturation rate (at 25 °C) shows that after pH 6 there is very little further effect of NTA on the degree of inhibition of barite precipitation (Fig. 6). The speciation curve suggests that by pH 12 the amount of NTA complexed is 90%, however, we must calculate the amount of barium ions complexed in order to ascertain the effect on supersaturation. The percentage of barium ions within a complex is 20% at this pH value. Despite this drop in free barium ions, the degree of inhibition appears

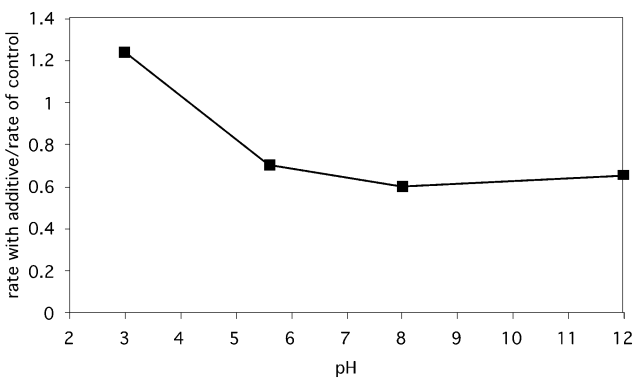

Fig. 6 Effect of 0.052 mM (10 ppm) NTA on barite precipitation conducted at various pHs and 25 °C.

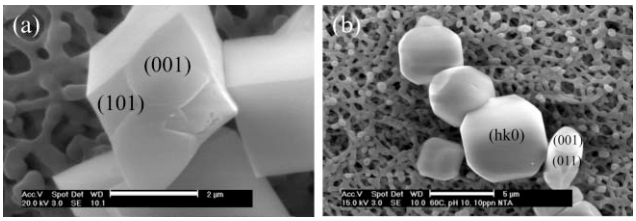

Fig. 7 Effect of pH with 0.052 mM NTA at 60 °C. (a) pH 7; (b) pH 10 (expected faces have been indicated assuming the (001) face is as presented, scale bars 2 μm).

relatively static. Given the ±10% error in this method this may be a sensitivity issue.

At the higher temperature of 60 °C, however, the pH appears to have a more dramatic impact (Fig. 7). In fact, as can be seen from both Fig. 5 and 7, as temperature increases, the NTA's ability to modify morphology decreases somewhat but improves slightly as pH goes up at the higher temperature. It is possible that acid may promote the degradation of NTA at higher temperatures but such information is not available and beyond the scope of this work. The supersaturation decreases at 298 K from ~25 to ~17 at 333 K,[21] thus the solubility has increased by 50% in a stoichiometric reaction (c_0 increases from 0.010 to 0.015 mM). Normally, as supersaturation decreases the effect of additives is increased rather than decreased.

The differences between room temperature and higher temperatures on NTA's ability to inhibit could be due to kinetic factors. That is, if the mode of inhibition is related to adsorption and desorption kinetics (that increase with temperature) then this would have a profound impact on the inhibition and/or morphology changes. In particular, if adsorption were an exothermic process then increases in temperature would increase the desorption reaction more significantly. In fact at pH 7 (and 60 °C) the morphology is reminiscent of barite formed at low supersaturation, thus at the higher temperature less NTA adsorption may be occurring. Even increasing the concentration to 0.26 mM NTA at pH 7 and 80 °C showed no significant difference in the morphology to that obtained at 0.052 mM.

Attempts were also made to follow the formation of particles (at RT) with time using TEM (when 0.26 mM NTA was present during barium sulfate precipitation). By sampling during and after the induction time (observed visually to be approximately 0.5 h) it was hoped that some light could be shed on how the particles evolve to their final shape. As can be seen from Fig. 8, precipitation begins as small, essentially spherical nanoparticles that agglomerate into larger spherical and ellipsoid shaped particles.

As precipitation proceeds, these aggregates become more crystalline (SAED shows distorted spots) with a roughly hexagonal shape. Essentially, then, we see round particles in the SEM pictures because these particles are harvested prior to ageing and ripening effects. Although the aged samples appear to be hexagonal they are also rounded as can be seen in the SEM pictures (ESI, Fig. S5).†

Several attempts were made to obtain an adsorption isotherm but data could not be reproducibly obtained (using infrared and thermogravimetric techniques). It is believed that

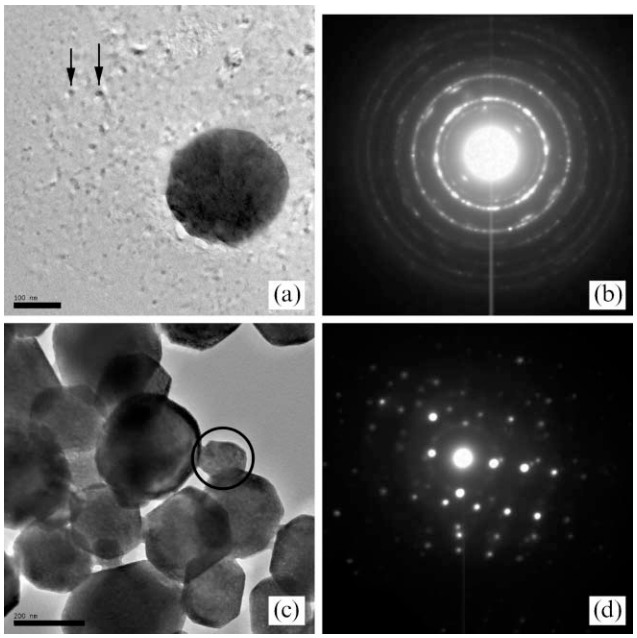

Fig. 8 Barium sulfate particles formed in the presence of 0.26 mM NTA at (a) 10 min (scale bar 100 nm) and (b) the SAED of the large particle in (a). Arrows in (a) show presence of even smaller particles, (c) aged particles of barite in the presence of 0.26 mM NTA (scale bar 200 nm) and (d) SAED of particle circled in (c).

carbonate (*via* adsorbed CO_2 from the atmosphere) interferes with the analysis of adsorbed NTA. This is not uncommon for carboxylate molecules and has been noted previously in the literature.[22] In addition, at higher levels of NTA, dissolution of the barite occurred, thus impeding any meaningful adsorption data being collected. Fourier transform infrared spectra were collected on both NTA solutions and barium sulfate slurries in the absence and presence of NTA at various pH values (25 °C). Fig. 9 shows that very little difference is observed in the solution spectra of NTA as the pH changes. A band at $\sim$1730 cm^{-1} is indicative of the C=O from the COOH group (absent in these spectra), while the 1430 cm^{-1} and 1600–1650 cm^{-1} bands have been assigned to the COO^- symmetric and asymmetric stretch, respectively.[18] In this work the asymmetric stretch appears at 1630–1640 cm^{-1} depending on pH. In the absence of barium cations, this lack of change with pH is to be expected.

When barium sulfate is present (Fig. 10), the 1630–1640 cm^{-1} band has shifted to $\sim$1600 cm^{-1}, and this is particularly noticeable at the higher pHs. This suggests that NTA chemisorbs onto the barium sulfate surface. It was found that the bands were consistent with COO–M bonds found in solid complexes as stated in the literature where M = Ba^{2+}.[23]

The band found at $\sim$1700 cm^{-1} in the adsorbed spectra is, in light of the modelling studies (see below), probably best interpreted as hydrogen bonding between the NTA molecule and the barium sulfate surface since the C=O is not expected to be present (from speciation data) and is lower in wavenumber than expected for the C=O stretch (1730 cm^{-1} discussed above). There are some other notable changes in the adsorbed spectra:

(i) there is a decrease in the band at $\sim$1360 cm^{-1} with increasing pH;

(ii) the band at $\sim$1330 cm^{-1} shifts to higher wavenumbers ($\sim$1340 cm^{-1}) with increasing pH.

These two bands are also associated with the COO^- anion according to ref. 23. Of more interest, perhaps, is that the shift to lower wavenumbers in the asymmetric stretch increases as pH increases. This suggests that chemisorption is greater at the higher pH values. Also, the difference between the wavenumber values of the asymmetric and symmetric stretches appears to decrease with an increase in pH and this may suggest a chelating bidentate structure between the carboxylate group and the barium cation.[24]

In order to understand the interactions occurring on a more fundamental level, molecular modelling was performed with and without the zwitterion formation. This was conducted in an effort to determine the impact (or otherwise) of the presence of the zwitterion. The zwitterion is expected to have the greatest effect when the functional group is not so tightly bound and our previous modelling on phosphonate inhibitors showed a very strong phosphonate group adsorption (if the functional group interaction is strong it will dominate the interaction and only small differences in the energy with and without zwitterion will be seen). Thus, carboxylate inhibitors were seen as a better candidate for this investigation. The NTA molecule without the zwitterion is the same LH^{2-} species but

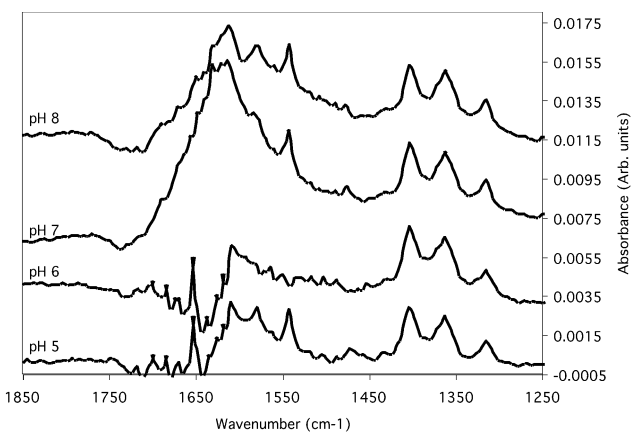

Fig. 9 HATR solution spectra of NTA at different pHs. Spectra have been offset for clarity.

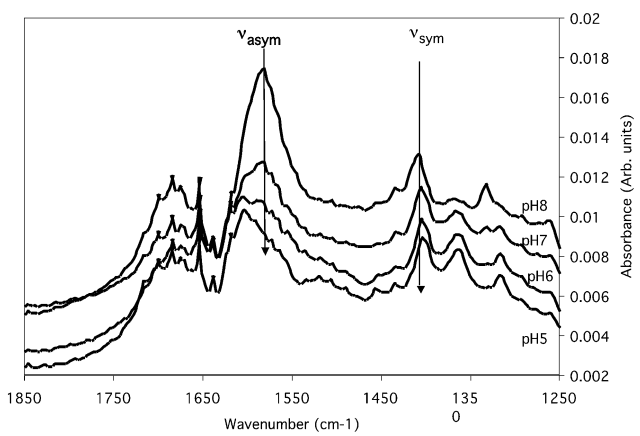

Fig. 10 HATR spectra of NTA adsorbed onto barium sulfate at various pHs. Spectra have been offset for clarity.

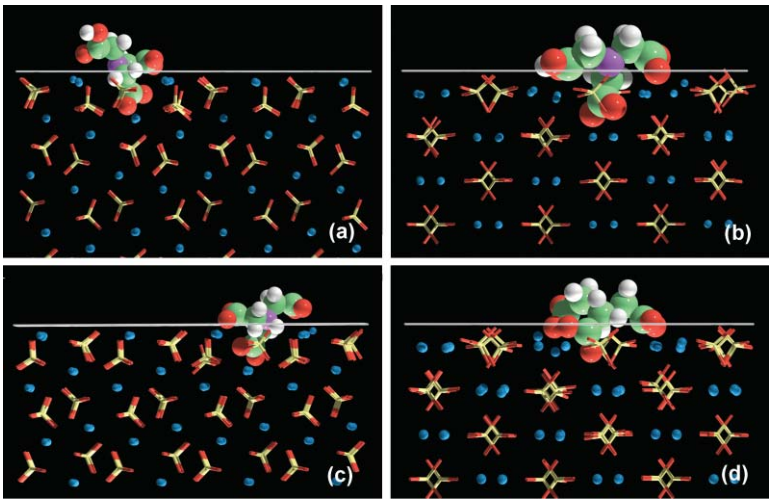

Fig. 11 Adsorption configurations for the two most favoured faces in order of decreasing adsorption energy, as viewed from a side perspective. (a) (100b) face, no zwitterion present; (b) (010) face, no zwitterion present; (c) (100b) face, zwitterion present; (d) (010) face, zwitterion present.

with one of the carboxylate groups protonated while the zwitterion form naturally has the proton bonded to the nitrogen atom. The trend in replacement energy (which gives an indication of the favourability of adsorption) was found (when not in zwitterion form) to be:

(100b) < (010) < (100a) < (101) < (011) < (211) < (001) < (210).

Note, the lower the replacement energy the more favourable adsorption will be. The (100) face has two possible terminations (see ref 16 for a more detailed discussion) and both have a favourable interaction with the NTA molecule. Fig. 11 shows the two most favoured configurations for adsorption.

In the case of the zwitterion being present, the following trend with replacement energy was found:

(100b) < (010) < (100a) < (211) < (011) < (101) < (001) < (210).

As can be seen, the presence of the zwitterion did not alter the most favoured faces for adsorption, nor the least favoured. The only difference between the two sets of simulations is the (211), (011) and (101) face ordering. The two most favourable adsorption configurations are shown in Fig. 11, and show that the main difference is that the hydrogen on the zwitterion is also able to interact *via* hydrogen bonding to the oxygen atoms on the sulfate groups. Most interestingly, the NTA with the protonated carboxylate *did not* show any hydrogen bonding on the (100b) face. This can be understood in terms of the strong Ba^{2+}–O_{NTA} interaction. The unprotonated oxygen on the carboxylate interacts with the surface barium ion and this forces the stereochemistry of the protonated oxygen atom away from the surface, such that no hydrogen bonding is possible. On the zwitterion molecule, all carboxylate groups are deprotonated, thus maximising this strong Ba^{2+}–O_{NTA} interaction but additionally, hydrogen bonding is also occurring. There is only one H bond at 1.7 Å (H_{zwit}–O_{sulf}), although three other interactions exist that are between 3 and 4 Å in length between the zwitterion hydrogen atom and the sulfate oxygen atoms. The presence of the zwitterion increased the magnitude of the replacement energy by ~100 kJ mol^{-1} for all of the faces studied (see Table 2) and made the process of adsorption more favourable. On some faces, the protonated carboxylate does hydrogen-bond but the zwitterion always has the lower replacement energy because it can both hydrogen-bond and maximise the Ba^{2+}–O_{NTA} interactions (*via* the slightly greater coloumbic attractions). In these cases the replacement energy difference is less than 100 kJ mol^{-1}. Clearly, hydrogen bonding does enhance the adsorption of additives when possible. This is in agreement with van der Leeden[25] who stated that the increased inhibitory action of HEDP (hydroxyethylenediphosphonic acid) was due to hydrogen bonding. In addition, it was found that the carboxylate groups (in the zwitterion form) are able to bond with the barium cations in both a bridging bidentate and a chelating bidentate mode[24] for the (100b) surface, where two of the carboxylate groups were in both a chelating and bridging structure (*i.e.* interacting with two barium ions one of which is in the chelate-type structure) while the third was found to be in a bridging-type structure only.

The presence of water on the barium sulfate surface is not expected to change the adsorption configuration significantly, however, it would undoubtedly influence the replacement energy since the NTA would have to displace some of this water (from molecular dynamics simulations[26] the adsorbed water has an adsorption energy of ~50 kJ mol^{-1}). However, this change would be small compared to the replacement energies reported here and might be compensated by hydrogen

Table 2 Replacement energy (kJ mol^{-1}) for the various $BaSO_4$ faces studied

Barite face (*hkl*)	NTA	NTA-zwitterion	% difference[a]
001	−437.86	−496.14	12
210	−332.56	−403.96	18
211	−446.35	−612.12	27
010	−852.07	−948.16	10
011	−522.72	−575.10	9
101	−541.27	−560.27	3
100b	−936.21	−1056.52	11
100a	−590.39	−685.71	14

[a] between NTA and NTA-zwitterion replacement energy (zwitterion used as reference)

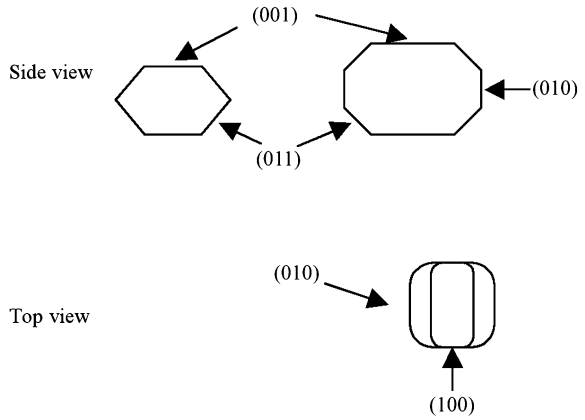

Scheme 1 Schematic showing assignment of faces based on the (001) face being assumed to be uppermost.

bonding between the NTA molecule with the remaining water molecules on the surface.

At room temperature and 0.052 mM NTA, the almost cube-like structures suggest that the side faces are actually (010) and (100) faces. However, at RT and 0.26 mM NTA any cube-like structure is difficult to determine. The main effect at the higher concentration has been to form much smaller particles. We can tentatively assign the faces of the nanoparticles (seen in Fig. 8c) as shown in Scheme 1.

The TEM thin sections showed that the particles were not of a uniform thickness but showed some porosity throughout while others showed clear signs of dissolution (Fig. 12). The substructure appearance of porosity has been previously observed and attributed to aggregated growth and ripening effects also related to dissolution and recrystallization.[27] After ageing all observed particles had the quasi-hexagonal structure. The particle shown in Fig. 12 was taken from an aged sample not ultramicrotomed, suggesting that the particle underwent some dissolution (experience with barium sulfate in the TEM suggests this extent of 'damage' is not due to the beam). TEM elemental analysis was unable to detect any nitrogen. Whether this is because the levels were below detection or because the NTA had dissolved from the structure is unknown.

The SAED patterns showed a variety of different diffraction patterns due to the rounded nature of the particles, however, the (010) zone and (100) zone could be identified (see ESI, Fig. S6)† on many occasions. What could definitely be excluded was the (210) face being present. We can confidently say that, due to the orthogonal nature of the particles, the two faces making the sides of the barite particles are the (010) and (100) faces, with some rounding also occurring. This finding supports the molecular modelling results discussed earlier.

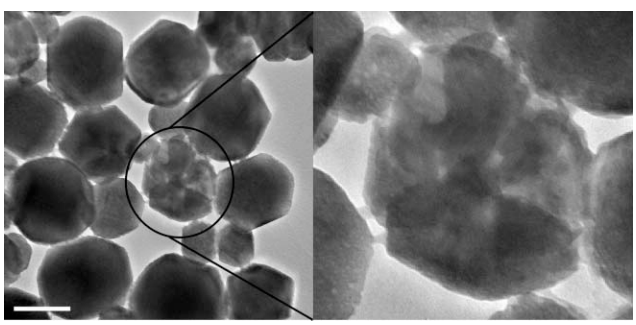

Fig. 12 TEM images of barium sulfate particles showing signs of dissolution having occurred. Inset shows higher magnification of the 'dissolved' particle. Scale bar is 200 nm in first picture.

Discussion

Carboxylate polymer molecules inhibit barium sulfate precipitation due to the large number of carboxylate–surface interactions,[28] but small carboxylate molecules are not generally recognised as inhibiting the precipitation of barium sulfate at moderate pHs where complexation is expected to be low. Morphology effects of small carboxylates have been reported at high pH and attributed to solution complexation.[8,9]

Clearly, from our previous work and this work, inhibition by the small NTA carboxylate occurs at moderate pHs and low concentrations, where complexation is expected to be negligible. The nephelometry results clearly indicate that the induction period of barium sulfate is affected by the presence of NTA. Since complexation is not a significant contributor to this system, it can be confidently assumed that this is not due to changes in the supersaturation of the solution. However, the adsorption of NTA onto barium sulfate as seen from the FTIR evidence means that there will be an effect on the barium sulfate surface free energy and, by inference, on the interfacial free energy. From nucleation theory[12] if the interfacial free energy increases, then the critical nucleus size is expected to decrease. Thus, the observed increase in induction time could be due to the longer time period required for the particles to grow to a size sufficient to be detected by the turbidity probe. However, the change in interfacial free energy also affects the nucleation rate ($J \propto A\exp\{-\gamma^3\}$).[12] Thus, an increase in the interfacial free energy can both reduce the critical nucleus size and reduce the nucleation rate, both leading to longer induction periods being observed.

The morphologies of the barium sulfate particles produced in the presence of NTA are almost identical at low and high pH at room temperature. Perhaps, it is not so much the amount of NTA–Ba complex that is important but the amount of NTA able to adsorb. Consider the following equilibrium:

$$LH^{2-} + Ba^{2+} \Leftrightarrow LHBa\ (complex) \qquad (1)$$

Even if the equilibrium lies almost completely to the right at high pH, if there is a small amount of the LH^{2-} species being lost to adsorption then the equilibrium will be shifted back towards the left slightly. The room temperature FTIR evidence has shown that chemisorption is stronger at the higher pHs. This may explain the lack of morphological differences between the pH 12 sample and pH 6 sample at 25 °C, *i.e.* the morphology is determined by the adsorbed NTA and this is occurring alongside the complex formation reaction.

Only at high temperatures do major differences in the morphology begin to be observed on altering pH. From the effect on morphology it is expected that NTA is less effective as an inhibitor at elevated temperatures. The effect of temperature is a difficult one to interpret since some important data are lacking (such as the decomposition at elevated temperature, adsorption at higher temperature, *etc.*). However,

given that the estimated log K values for NTA at 60 °C suggests that almost all of the NTA is complexed with barium at pH 10 (see ESI, Fig. S2),† we would expect the morphology at pH 10 to be most like that observed at pH 7. Without further information (which we hope to gather in the future) the simplest explanation is one of kinetics; the crystallization kinetics are faster at higher temperatures and this may mean that the adsorption of NTA is much slower in comparison and so its effect is weakened.

The molecular modelling shows that the (100) face of barite was the most favourable for adsorption. This interaction was observed experimentally at room temperature but is not observed at pH 7 and higher temperatures. In the case of the zwitterion, it was found from modelling that the main interaction of NTA is through the carboxylate group but that a small additional driver to adsorb in the presence of the zwitterion is *via* hydrogen bonding with surface oxygen atoms.

At room temperature and very high concentrations of NTA, nanoparticles are formed that are observed to aggregate together. On ageing, the aggregates undergo an ageing/ripening process that is probably occurring *via* dissolution and re-precipitation.

Conclusions

In conclusion, the small aminocarboxylate NTA has a significant impact on barium sulfate crystallization provided the carboxylate groups are deprotonated. It has been shown that NTA adsorbs onto barium sulfate and that NTA is able to influence the induction time of barium sulfate crystallization. We conclude that the modification of the induction time is caused by NTA adsorption onto the critical nuclei and this alters the interfacial free energy. This is supported by infrared data and molecular modelling results showing NTA can and does adsorb onto barium sulfate.

At higher temperatures NTA does not affect the morphology to the same degree as at room temperature. This is not considered to be an issue of decomposition but is more likely a result of kinetics. The pH is seen to be more important for the ability of NTA to alter the barite morphology at elevated temperatures, however, the effect on morphology is not that expected from the speciation data (at 60 °C). It is predicted from the speciation data that NTA should be fully complexed to barium cations, yet the morphology is not that expected from a lower free barium cation activity. Future work to determine NTA adsorption (at least qualitatively) at this temperature is planned.

Molecular modelling has shown that the NTA can chemisorb onto several faces of barium sulfate and the most favoured faces for adsorption are those observed experimentally in the room temperature results at higher concentrations ($>$0.052 mM). The presence of the zwitterion did not alter the preference for NTA to adsorb onto the (100) and (010) faces, but it did change the replacement energy such that it became more favourable. This was found to be due to hydrogen bonding that occurred when the proton was positioned on the nitrogen atom rather than the carboxylate group.

In the presence of NTA at very high concentrations ($\geqslant$0.26 mM) found that spherical nanoparticles are formed which agglomerate (forming a polycrystalline product) and eventually ripen to a more hexagonal shape.

As a final cautionary note, it is perhaps important that although these small molecules are known as complexing agents, their actual mode of interaction should be determined using complementary techniques. Only then can we fully comprehend the morphology modification mechanism and use this knowledge for particle engineering purposes.

Acknowledgements

The authors gratefully acknowledge that this research has been supported under the Australian Government's Cooperative Research Centre (CRC) Program, through the AJ Parker CRC for Integrated Hydrometallurgy Solutions. We would also like to thank John Murphy of UWA's Centre for Microscopy and Microanalysis for preparing the ultramicrotomed samples.

References

1 M. P. Pileni, J. Tanori and A. Filankembo, *Colloids Surf., A*, 1997, **123–124**, 561.
2 L.-Q. Wu, K. Lee, X. Wang, D. S. English, W. Losert and G. F. Payne, *Langmuir*, 2005, **21**, 3641.
3 H. Cölfen and S. Mann, *Angew. Chem., Int. Ed.*, 2003, **42**, 2350.
4 I. Weissbuch, L. Leiserowitz and M. Lahav, in *Crystallization Technology Handbook*, ed. A. Mersmann, 1995, Marcel Dekker Inc., New York, ch. 6, p. 401.
5 N. Loges, K. Graf, L. Nasdala and W. Tremel, *Langmuir*, 2006, **22**, 3073.
6 H.-C. Schwarzer and W. Peukert, *Chem. Eng. Technol.*, 2002, **25**(6), 657.
7 K. S. Sorbie and E. J. Mackay, *J. Petroleum Sci. Eng.*, 2000, **27**, 85.
8 M. Uchida, A. Sue, T. Yoshioka and A. Okuwaki, *J. Mater. Sci. Lett.*, 2000, **19**, 1373.
9 M. Uchida, A. Sue, T. Yoshioka and A. Okuwaki, *CrystEngComm*, 2001, **5**, 1.
10 F. Jones, J. Clegg, A. Oliveira, A. L. Rohl, M. I. Ogden and G. M. Parkinson, *CrystEngComm*, 2001, **40**, 1.
11 N. Gabas, N. Hiquily and C. Laguérie, *Part. Part. Syst. Charact.*, 1994, **11**(2), 121.
12 J. W. Mullin, in *Crystallization*, Butterworth-Heinemann, Oxford, UK, 3rd edn, 1993, ch. 5, p. 172.
13 F. Jones and A. L. Rohl, *Mol. Simul.*, 2005, **31**(6–7), 393.
14 S. D. Fleming and A. L. Rohl, *Z. Kristallogr.*, 2005, **220**(5–6), 580.
15 J. D. Gale and A. L. Rohl, *Mol. Simul.*, 2003, **29**(5), 291.
16 F. Jones, W. R. Richmond and A. L. Rohl, *J. Phys. Chem. B*, 2006, **110**, 7414.
17 F. Jones, A. L. Rohl, J. B. Farrow and W. van Bronswijk, *Phys. Chem. Chem. Phys.*, 2000, **2**, 3209.
18 E. R. Souaya, W. G. Hanna, E. H. Ismail and N. E. Milad, *Molecules*, 2000, **5**, 1121.
19 T. P. Knepper, *TrAC, Trends Anal. Chem.*, 2003, **22**(10), 708.
20 F. Jones, A. Oliveira, G. M. Parkinson, A. L. Rohl, A. Stanley and T. Upson, *J. Cryst. Growth*, 2004, **262**, 572.
21 *Solubilities of inorganic compounds*, ed. H. Stephen and T. Stephen, Pergamon Press, London, 1979, vol. 1 part 1, 157.
22 K. D. Dobson and A. J. McQuillan, *Spectrochim. Acta, Part A*, 1999, **55**(7–8), 1395.
23 F. J. M. Rajabalee, *Spectrochim. Acta, Part A* , 1974, **30**, 891.
24 F. Jones, J. B. Farrow and W. van Bronswijk, *Langmuir*, 1998, **14**(22), 6512.
25 M. C. van der Leeden, PhD Thesis, Technical University of Delft, Delft, 1991.
26 S. Piana, F. Jones and J. D. Gale, *J. Am. Chem. Soc.*, DOI: 10.1021/ja064706.
27 B. Judat and M. Kind, *J. Colloid Interface Sci.*, 2004, **269**, 341.
28 P. J. Breen, H. H. Downs and B. N. Diel, *Spec. Publ. - R. Soc. Chem.*, 1991, **97**, 186.

